

Stable water isotopologue fractionation during soil-water evaporation: Analysis using a coupled soil-atmosphere model

Stefanie Kiemle¹, Katharina Heck¹, Edward Coltman¹, Rainer Helmig¹

¹Institute for Modelling Hydraulic and Environmental Systems, Department of Hydromechanics and
Modelling of Hydrosystems, University of Stuttgart, Stuttgart, Germany

Key Points:

- Stable water isotopologue distribution in the unsaturated zone
- Coupled soil-atmosphere models
- Isotopic fractionation processes during evaporation

Corresponding author: Stefanie Kiemle, stefanie.kiemle@iws.uni-stuttgart.de

Abstract

[Stable water isotopologues tend to fractionate from ordinary water during evaporation processes resulting in an enrichment of the isotopic species in the soil. The fractionation process can be split into equilibrium fractionation and kinetic fractionation. Due to the complex coupled processes involved in simulating soil-water evaporation accurately, defining the kinetic fractionation correctly remains an open research area. In this work, we present a multi-phase multi-component transport model that resolves flow through both the near surface atmosphere and the soil, and models transport and fractionation of the stable water isotopologues using the numerical simulation environment DuMu^x. Using this high resolution coupled model, we simulate transport and fractionation processes of stable water isotopologues in soils and the atmosphere without further parameterization of the kinetic fractionation process as is commonly done.

In a series of examples, the transport and distribution of stable-water isotopologues are evaluated numerically with varied conditions and assumptions. First, an unsaturated porous medium connected to constant laminar flow conditions is introduced. The expected vertical isotope profiles in the soil as described in literature are reproduced. Further, by examining the spatial and temporal distribution of the isotopic composition, is determined the enrichment of the isotopologues in soil is linked with the different stages of the evaporation process. Building on these results, the robustness of the isotopic fractionation in our model is analysed by isolating single fractionation parameters. The effect of wind velocity and turbulent atmospheric conditions is investigated, leading to different kinetic fractionation scenarios and varied isotopic compositions in the soil.

]

1 Introduction

Stable water isotopologues are commonly used as natural tracers to determine the water movement within the unsaturated zone (e.g. Sprenger et al., 2016, 2018). Analyzing their compositions in water has proven to be a suitable tool for better understanding evaporation and mixing processes within soils and at the soil-atmosphere interface. For instance, the location of the evaporation front within the soil can be identified by measuring the isotopic composition (Rothfuss et al., 2015). During evaporation, stable water isotopologues are affected by fractionation processes. In soil-atmosphere systems this process can be divided into equilibrium and kinetic fractionation (Craig, 1961; Craig & Gordon, 1965). Due to their differences in vapor pressure (equilibrium fractionation) and their varied diffusion coefficients (kinetic fractionation), the transport and flow behavior of stable water isotopologues is different in comparison to ordinary water.

Whereas the description of the equilibrium fractionation is consistent in literature (Majoube, 1971; Horita & Wesolowski, 1994; Luz et al., 2009), in terms of the kinetic fractionation, there are uncertainties in defining the relationship between the vapor diffusion coefficients under evaporating conditions (e.g. Quade et al., 2018; Luz et al., 2009). The major challenge in determining the kinetic fractionation correctly is how to include the influence of the atmosphere under different wind velocities (Quade et al., 2018).

In the past, many one-dimensional process-based models have been developed: ODWISH (Shurbaji & Phillips, 1995), MOISE (Mathieu & Bariac, 1996; Melayah et al., 1996), SiSPAT-Isotope (Braud et al., 2005), Soil-Litter-Iso (Haverd & Cuntz, 2010), HYDRUS isotope module (Stumpp et al., 2012), SWIS (Müller et al., 2014; Sprenger et al., 2018), HYDRUS-1D (Zhou et al., 2021). With these 1D model approaches, fractionation processes within the unsaturated zone and in the interface region can be simulated. However, these models only cover the influence of the free-flow domain by including evaporation boundary conditions and using parameterizations to describe the kinetic fractionation. Thus, the influence of the free flow on the fractionation process can only be modeled for certain conditions where suitable parameterizations are available. Additionally, the spatial dis-

tribution of the isotopologues is only analyzed in 1D, and possible multidimensional effects cannot be analyzed with these models.

Concerning multi-dimensional isotopologue transport models in the subsurface, some models can be found in literature: TAC^D (Uhlenbrook et al., 2004), NASA-Giss ModelE (Aleinov & Schmidt, 2006), CMF (Kraft et al., 2011; Windhorst et al., 2014), ECHAM5-JSBACH-wiso (Haese et al., 2012), ORCHIDEE (Risi et al., 2016), iCLM4 (Wong et al., 2017), EcoH2O-iso* (Kuppel et al., 2018), TOUGH2 (Jiang et al., 2018). However, besides the issue that these models operate on a larger scale with lower resolution (land surface or catchment models) than our target scale, they also rely on parameterizations to describe the isotope transport and fractionation. Further, none of these models include the influence of atmospheric flow on the isotopic fractionation processes in the porous-medium domain by accounting for the flow and transport in the free-flow domain and coupling the free-flow to the porous-medium domain. To our knowledge, there is no stable water isotopologue transport model, which resolves both domains and couples the free-flow and the porous-medium domain.

In the following, we present a multi-dimensional stable water isotopologue transport model which couples a free-flow domain and a porous-medium domain and ensures mass, momentum, and energy conservation. Evaporation of both ordinary water and isotopologues can be described under varying free-flow conditions, e.g., varying wind speeds including turbulent and laminar flow conditions. This means we can describe the fractionation process in the free-flow domain, the interface region, and the porous-medium domain without implementing the commonly used fractionation parameterizations. This allows us to analyze the flow and transport of the isotopologues together with the evaporation process of ordinary water. Further, the influence of the different stages of the evaporation processes on isotopologue behavior can be reviewed. It also allows us to isolate physical factors, analyzing the processes contributing to isotopologue fractionation independently.

2 Methods

In this section, we describe the principles of fractionation processes of stable water isotopologues during evaporation from soils (Section 2.1), as well as the applied coupled model concept (Section 2.2). This model concept includes the description of mass and energy transfer within the porous-medium domain Ω_{pm} , within the atmospheric free-flow domain Ω_{ff} , and the coupling concept connecting the domains. At the end of the chapter, the numerical model is briefly explained in Section 2.3.

2.1 Fractionation Processes of Stable Water Isotopologues

Craig and Gordon (1965) proposed a model for isotopic effects during evaporation from a free water surface. The so-called Craig-Gordon model describes the effects of the different transport mechanisms and fractionation processes between the water surface and the ambient air.

The original Craig-Gordon model is distributed into three zones. These zones can be adapted for the application in porous medium by extending the zones to the soil-water evaporation front. These zones are as follows: (1) a turbulent zone where turbulent mixing occurs and the isotopic composition becomes constant; (2) a diffusive zone defined by the viscous sub-layer where diffusive transport dominates and kinetic fractionation is the leading fractionation process; and (3) an interface zone where the liquid and vapor phase are in isotopic equilibrium inside the porous medium and equilibrium fractionation governs the fractionation process. In Figure 1, the isotopic composition profile and the classification into the specific fractionation zone are illustrated.

Analyzing the enrichment of isotopic species in soils can be used to determine the depth or progression of the evaporation front in unsaturated soils. The evaporation front can be located at the maximal gradient of the isotopic composition (Rothfuss et al., 2015). This and the impact of the different evaporation stages on the enrichment process are depicted in Figure 1.

During stage-I evaporation (Figure 1a), the atmospheric evaporation potential is satisfied at the soil-atmosphere interface by capillary recharge. As the soil dries out further, the evaporation rate reduces as stage-II evaporation begins (Figure 1b) (e.g. Lehmann et al., 2008). Here, liquid water at the interface is no longer mobile and evaporation is possible through diffusive transport. While the soil dries out, the position of the isotopic zones rearranges. The interface zone, characterized by equilibrium fractionation, moves with the evaporation front downwards, and the diffusive zone, characterized by kinetic fractionation, is thereby extended. The maximal gradient of the isotopic composition and so the evaporation front is no longer located at the porous-medium domain surface, but below the soil surface, in the transition between the diffusive and interface zone.

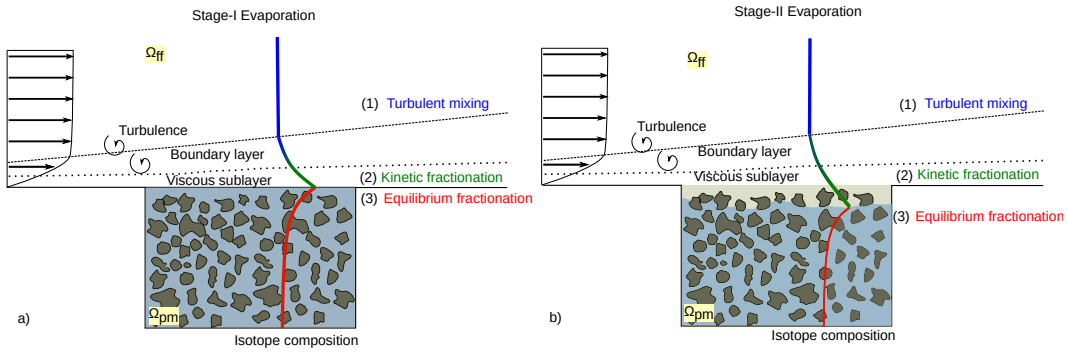


Figure 1: Isotopic composition profiles during (a) stage-I evaporation, (b) stage-II evaporation and the classification into their respective isotopic fractionation processes.

The main driving processes for isotopic fractionation in soils and at the soil-atmosphere interface are commonly expressed by the equilibrium fractionation factor and the kinetic fractionation factor. These factors are normally expressed by the symbol α . However, to avoid misunderstandings with the definition of the subscripts α describing the phases, we denote the fractionation factors in the following with β . In general, the fractionation factor describes the tendency of two components κ to separate from its mixture.

The isotopic equilibrium fractionation factor β_{eq}^i describes the phase equilibrium between liquid and gaseous phases for water and its isotopologues (Majoube, 1971; Van Hook, 1968),

$$\frac{x_l^i}{x_{H_2O}^i} \beta_{eq}^i = \frac{x_g^i}{x_{H_2O}^i}, \quad (1)$$

with x denoting the mole fraction of a component $\kappa \in \{i, H_2O\}$. Here, the i stands for the heavier isotopologues while H_2O denotes ordinary water. Phase indices are denoted by the subscript α in general and specifically with l for the liquid phase and g for the gaseous phase.

The equilibrium fractionation factor is defined by the different vapor pressures of the isotopologues p_g^i and ordinary water $p_g^{H_2O}$ and is commonly expressed by the depen-

dence on the temperature T and coefficients that can be chosen from literature:

$$\beta_{eq}^i = \frac{p_g^i}{p_{H_2O}^{H_2O}} = \exp\left(-\left(\frac{A}{T^2} + \frac{B}{T} + C\right)\right). \quad (2)$$

With this definition, the equilibrium fractionation factor is smaller than 1, which leads to the enrichment of the isotopologues in liquid water compared to ordinary water. More information about the used coefficients can be found in Section 3.

For the kinetic fractionation factor, which describes the fractionation of isotopic species caused by the difference in diffusive transport of water and its isotopologues, many approaches exist. Barnes and Allison (1984) described the kinetic fractionation factor considering only molecular transport. Dongmann et al. (1974) (see Eq. 3) extended the definition of Barnes and Allison (1984) by involving free-flow properties. Besides these definitions Brutsaert (1975), Mathieu and Bariac (1996), Gat (1971), Craig and Gordon (1965), Quade et al. (2018) published alternative formulations. The kinetic fractionation factor is commonly described by the diffusion coefficients D :

$$\beta_{kin}^i = \left(\frac{D_{H_2O}^{H_2O}}{D_g^i}\right)^n. \quad (3)$$

In the above-described literature, the exponent n varies depending on the free-flow conditions (turbulent or laminar). However, the fully resolved coupled model does not use a kinetic fractionation factor. This factor is implicitly included in the model via their different diffusion coefficients used in the transport equations in both the free-flow and the porous-medium domains. In Section 3, details about the diffusion coefficients used can be found.

In the coupled model, equilibrium and diffusive fractionation effects are described by solving two-phase four-component transport equations in the porous medium and one-phase four-component transport equations in the free-flow domain. Both domains are coupled with the help of suitable coupling conditions that ensure mass, momentum, and energy conservation.

In the following model concepts for the porous-medium domain, the free-flow domain, and the coupling conditions are presented.

2.2 Coupled Model Concepts

Porous-Medium Domain

The porous-medium flow domain is described by a multiphase Darcy's law in combination with a mass and energy balance to describe non-isothermal, multiphase flow. The mass balance equation for the component transport is written as the following:

$$\sum_{\alpha \in \{l, g\}} \left(\phi \frac{\partial (\rho_\alpha S_\alpha X_\alpha^\kappa)}{\partial t} + \nabla \cdot \mathbf{v}_\alpha \rho_\alpha X_\alpha^\kappa + \sum_{\kappa} \nabla \cdot (\mathbf{D}_{pm, \alpha}^\kappa \rho_\alpha \nabla X_\alpha^\kappa) \right) = 0, \quad (4)$$

here $\mathbf{D}_{pm, \alpha}^\kappa$ denotes the effective binary diffusion coefficient in the porous medium. Phase saturations are denoted by S_α and ρ_α is the density of the phase. X_α^κ is the mass fraction that is defined by $X_\alpha^\kappa = x_\alpha^\kappa \frac{M^\kappa}{M_\alpha}$ with M^κ as the molar mass of the component and M_α as the average molar mass of the phase. The fluid phase velocity \mathbf{v}_α is determined by Eq. 5:

$$\mathbf{v}_\alpha = -\frac{k_{r,\alpha}}{\mu_\alpha} K (\nabla p_\alpha - \rho_\alpha \mathbf{g}). \quad (5)$$

K denotes the intrinsic permeability of the porous medium and $k_{r,\alpha}$ the relative permeability of the phase. μ_α is the dynamic viscosity of the phase. Gravity is denoted by the vector \mathbf{g} . Within the porous-medium domain we assume a local thermodynamic equilibrium. The energy balance is defined by:

$$\sum_{\alpha \in \{l, g\}} \left(\phi \frac{\partial (\rho_\alpha S_\alpha u_\alpha)}{\partial t} + \nabla \cdot (\rho_\alpha h_\alpha \mathbf{v}_\alpha) \right) + (1 - \phi) \frac{\partial (\rho_s c_{p,s} T)}{\partial t} - \nabla \cdot (\lambda_{pm} \nabla T) = 0. \quad (6)$$

u_α is the internal energy of the phase and h_α the specific enthalpy. Due to the differences in enthalpies of the gaseous and the liquid phase, latent heat of vaporization is included in this approach. The solid part of the porous medium is accounted for by the specific heat capacity $c_{p,s}$ and the density of the solid ρ_s . The thermal conductivity λ_{pm} is a mixture of the thermal conductivities of the liquid and the gaseous and the solid phase and is computed by the Somerton approach (Somerton et al., 1974).

Free-Flow Domain

The free flow can be described by the Navier-Stokes equations:

$$\frac{\partial \rho_g \mathbf{v}_g}{\partial t} + \nabla \cdot (\rho_g \mathbf{v}_g \mathbf{v}_g^T) - \nabla \cdot (\boldsymbol{\tau}_g) + \nabla \cdot (p_g \mathbf{I}) - \rho_g \mathbf{g} = 0. \quad (7)$$

with \mathbf{I} as the identity matrix. The mass balance for each component is given by:

$$\frac{\partial (\rho_g X_g^\kappa)}{\partial t} + \nabla \cdot (\rho_g \mathbf{v}_g X_g^\kappa - \mathbf{j}_{\text{diff}}^\kappa) - q^\kappa = 0. \quad (8)$$

The diffusive fluxes $\mathbf{j}_{\text{diff}}^\kappa = \mathbf{D}_\alpha^\kappa \rho_\alpha \nabla X_\alpha^\kappa$ are, as in the porous medium, described by Fick's law.

In order to properly describe turbulent free-flow behaviour the so-called Reynolds-Averaged Navier-Stokes (RANS) equations are used. This splits the fluctuating terms into averaged and fluctuating values, which introduces a new term, the Reynolds stress tensor $\boldsymbol{\tau}_{g,t}$. The momentum balance then can be denoted as:

$$\frac{\partial \rho_g \mathbf{v}_g}{\partial t} + \nabla \cdot (\rho_g \mathbf{v}_g \mathbf{v}_g^T) - \nabla \cdot (\boldsymbol{\tau}_g + \boldsymbol{\tau}_{g,t}) + \nabla \cdot (p_g \mathbf{I}) - \rho_g \mathbf{g} = 0. \quad (9)$$

As closure relations for the newly introduced Reynold's stress $\boldsymbol{\tau}_{g,t} = \mu_{g,t} (\nabla \mathbf{v}_g + \nabla \mathbf{v}_g^T) - (\frac{2}{3} \rho_g k \mathbf{I})$ in this work a $k-\omega$ turbulence model is used. More information about this can be found in Wilcox (2008).

The mass balance equation for the transport of a component in the free flow is given with:

$$\frac{\partial (\rho_g X_g^\kappa)}{\partial t} + \nabla \cdot (\rho_g \mathbf{v}_g X_g^\kappa - \mathbf{j}_{\text{diff},t}^\kappa) - q^\kappa = 0. \quad (10)$$

where the turbulent diffusion $\mathbf{j}_{\text{diff},t}^\kappa$ uses an effective diffusion coefficient that also accounts for turbulent behaviour with: $D_{\text{eff},t}^{ij} = D_g^{ij} + D_t$. D_t is the eddy diffusivity.

The energy balance can be described with:

$$\frac{\partial (\rho_g u_g)}{\partial t} + \nabla \cdot (\rho_g h_g \mathbf{v}_g) + \sum_i \nabla \cdot (h_g \mathbf{j}_{\text{diff},t}^\kappa) - \nabla \cdot ((\lambda_g + \lambda_t) \nabla T) = 0, \quad (11)$$

where the λ_t is the eddy conductivity. More information about these models can be found in e.g. Fetzner et al. (2016).

Interface Coupling Conditions

The interface conditions are based on the assumption of local thermodynamic equilibrium (Mosthaf et al., 2011). At the interface we assume that temperatures, the pressure and mole fractions are equal. Continuity of fluxes at the interface is then described by:

$$[(\rho_g \mathbf{v}_g) \cdot \mathbf{n}]^{\text{ff}} = -[(\rho_g \mathbf{v}_g + \rho_w \mathbf{v}_w) \cdot \mathbf{n}]^{\text{pm}}. \quad (12)$$

The tangential component of the momentum balance is set to the Beavers-Joseph-Saffman condition (Beavers & Joseph, 1967; Saffman, 1971; Jones, 1973), describing the slip velocity at the interface.

$$\left[\left(-\mathbf{v}_g - \frac{\sqrt{(\mathbf{K} \mathbf{t}_i) \cdot \mathbf{t}_i}}{\alpha_{BJ}} (\nabla \mathbf{v}_g + \nabla \mathbf{v}_g^T) \mathbf{n} \right) \cdot \mathbf{t}_i \right]^{\text{ff}} = 0, \quad i \in \{1, \dots, d-1\}. \quad (13)$$

For the normal part of the momentum coupling condition, we use a continuity of normal stresses.

$$[(\rho_g \mathbf{v}_g \mathbf{v}_g^T - (\boldsymbol{\tau}_g + \boldsymbol{\tau}_{g,t}) + p_g \mathbf{I}) \mathbf{n}]^{\text{ff}} = [(p_g \mathbf{I}) \mathbf{n}]^{\text{pm}}. \quad (14)$$

For a component, i , continuity of fluxes is written as:

$$[(\rho_g X_g^\kappa \mathbf{v}_g + \mathbf{j}_{\text{diff},t}) \cdot \mathbf{n}]^{\text{ff}} = - \left[\left(\sum_{\alpha} (\rho_{\alpha} X_{\alpha}^{\kappa} \mathbf{v}_{\alpha} + \mathbf{j}_{\text{diff},\alpha}^{\kappa}) \right) \cdot \mathbf{n} \right]^{\text{pm}}. \quad (15)$$

For the energy coupling the flux condition is:

$$\left[\left(\rho_g h_g \mathbf{v}_g + \sum_i h_g^{\kappa} \mathbf{j}_{\text{diff},g}^{\kappa} + \lambda_g \nabla T \right) \cdot \mathbf{n} \right]^{\text{ff}} = - \left[\left(\sum_{\alpha} (\rho_{\alpha} h_{\alpha} \mathbf{v}_{\alpha} + \sum_i h_{\alpha}^{\kappa} \mathbf{j}_{\text{diff},\alpha}^{\kappa}) - \lambda_{\text{pm}} \nabla T \right) \cdot \mathbf{n} \right]^{\text{pm}}. \quad (16)$$

2.3 Numerical Model

The porous-medium domain is discretized using cell-centered finite volumes. The simulations were performed using a two-point flux approximation on a rectangular grid. The free-flow domain is also discretized using finite volumes but with the marker and cell scheme. More details are described in (Coltman et al., 2020).

The above-mentioned concepts are implemented using the open-source simulation environment DuMu^x (Koch et al., 2021; Flemisch et al., 2011), which is based on the open-source numerical toolbox DUNE. The source code for the below-performed simulations is accessible via a DuMu^x publication module (?, ?).

3 Simulation Scenario

In our analysis we investigated the fractionation behaviour of the heavy water isotopologues $^1H^2HO$ and $H_2^{18}O$ in relation to the lighter ordinary water H_2O during an evaporation process.

Therefore, we created a virtual evaporation case in which a partially-saturated soil column dries out under constant atmospheric conditions. The setup comprises a wind tunnel with a flat porous medium beneath. The wind velocity profile develops from the

left to the right side from a parabolic-shaped profile into a fully developed velocity profile. From the left side, the free-flow domain is constantly supplied with stable water isotopologues and water vapor. Figure 2 shows a sketch for the initial and boundary conditions of the simulation setup. As this evaluation does not include any specific pore scale information, the Beavers-Joseph coefficient α_{BJ} , used in the tangential momentum coupling condition, is set to 1.

Inside the porous-medium domain, we used a light clay (Yolo light clay ((Moore, 1937))) with a texture of 31.2 % clay, 45.0 % silt and 23.8 % sand for our simulations. The spatial parameters of the used soil are listed in Table 1.

The applied fluid system comprises the components *air*, H_2O , $^1H^2HO$ and $H_2^{18}O$. The non-isotopic properties and relationships of our fluid system can be found in (IAPWS, 2007), as well as in the DuMu^x documentation and in the DuMu^x publication module (git.iws.uni-stuttgart.de/dumux-pub/Kiemle2022a). The binary liquid diffusion coefficient for " H_2O - isotopologue" is proportional to the liquid self-diffusion coefficient of H_2O . The proportional factor can be found in Mathieu and Bariac (1996). The diffusion between air-isotopologues in the vapor phase was defined by using the gas diffusion coefficient of H_2O -Air and a proportional factor given by Merlivat (1978). The isotopic vapor pressure (see Eq. 2) was defined by using coefficients proposed by Van Hook (1968).

The composition of isotopologues is commonly written in the δ notation that relates the ratio of isotopologues to ordinary water to a standard value: $\delta_\alpha^i = \frac{R_\alpha^i - R_{V-SMOW}}{R_{V-SMOW}}$. 1000[‰] with $R_\alpha^i = \frac{N^i}{N^w}$ and R_{V-SMOW} the standard mean ocean water (Gonfiantini, 1978). Concerning the δ -notation, the superscript i describes only the heavier atom of the isotopologue instead of the entire molecule.

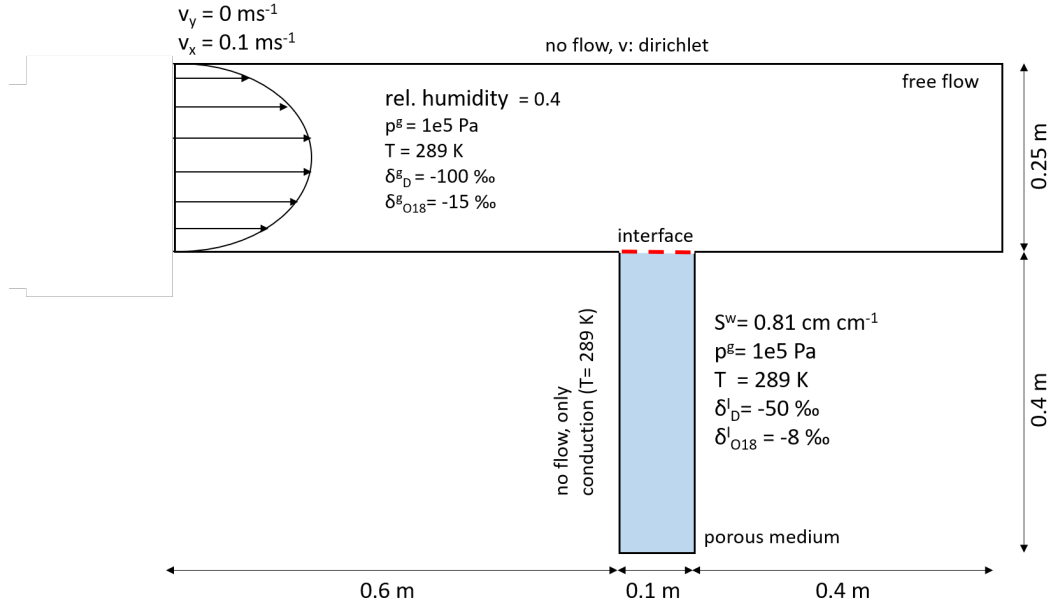


Figure 2: Initial and boundary conditions for analysing stable water isotopic fractionation during evaporation. The problem is discretized using 100 cells/m in the vertical direction and with 400 cells/m (porous-medium domain) and 100 cells/m (free-flow domain) in the horizontal direction. A vertical grid refinement towards the interface region is used.

Table 1: Spatial parameters of Yolo light clay

Parameter	Value
Porosity ϕ	0.35
Permeability K	1.23E-14 m ²
Residual saturation of non-wetting phase S_{nr}	0.00
Residual saturation of wetting phase S_{wr}	0.00
Van Genuchten parameter n	2.221
Van Genuchten parameter α	0.0005 Pa ⁻¹
Solid density ρ_s	1300 kg m ⁻³
Solid thermal conductivity λ_{pm}	0.5 W m ⁻¹ K ⁻¹
Solid heat capacity $c_{p,s}$	1300 J kg ⁻¹ K ⁻¹

4 Results and Discussion

In the following analysis, we set up a series of examples to investigate the transport and distribution of stable water isotopologues during the evaporation of the unsat-

urated porous medium. Using laminar flow conditions, we show that the spatial and temporal distribution of the isotopic composition match with the description in literature (Section 4.1), and by isolating single fractionation parameters, we highlight the robustness of our fractionation model (Section 4.2). Additionally, we present the variety of our coupled model by changing wind velocity and turbulent atmospheric conditions (Section 4.3).

4.1 Water isotopologue transport under laminar flow conditions

We focus on the fractionation behaviour in the porous-medium domain during the evaporation of a soil column. As described in Section 2.1, we expect an enrichment of isotopologues towards the evaporation front in the porous-medium domain caused by the equilibrium fractionation factor in the saturated zone and subsequently a decrease in the isotopic composition caused by intrusion of the isotopic-depleted atmosphere in the dried porous-medium zone. Thus the resulting isotope profile remains constant in the saturated zone (no fractionation), but forms a peak-shape at the evaporation front.

As a first step, we set up a stable water isotopologue transport problem with laminar flow ($v_x = 0.1$ m/s) above the porous-medium domain. Here, focus is placed on the isotope fractionation process itself without the influence of turbulent mixing in the free flow. In Figure 3, the isotopic compositions for various days are plotted as (a) vertical and (b) horizontal profiles. In the vertical profiles, it can be observed that the simulated profiles match the theoretical description depicted in Figure 1. Both, the isotopic enrichment towards the evaporation front and the depletion in the dry domain of the porous medium are simulated. Further, we observe how the soil column dries out over time as the evaporation front propagates downwards.

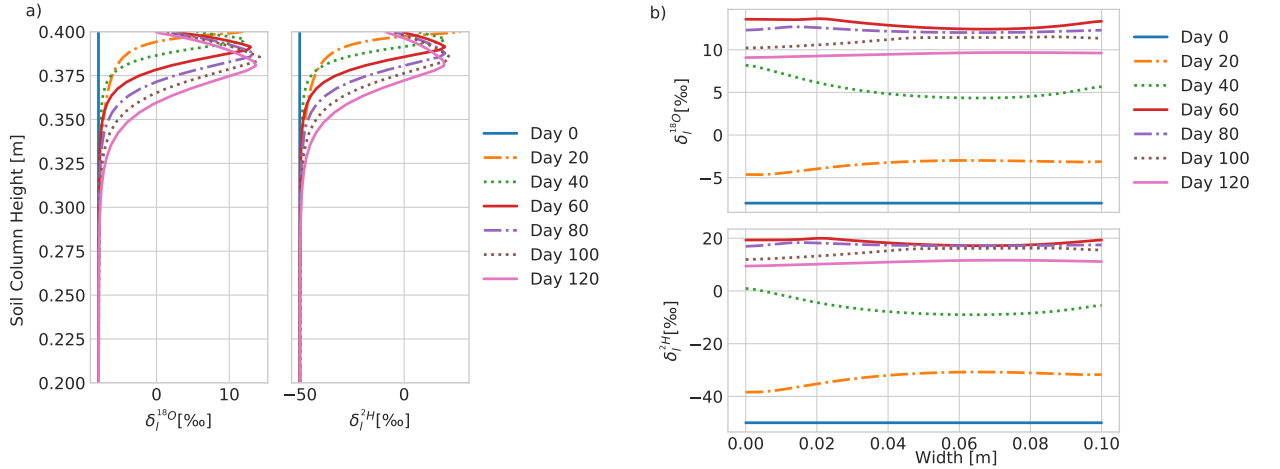


Figure 3: Isotopic composition δ_t^i over time. (a) Vertical relative concentration profile in the middle of the soil column at selected days; (b) horizontal relative concentration profile at 0.39 m soil column height at selected days.

In the horizontal profiles, the spatial distribution across the x-axis of the isotopologues and their fractionation behavior are visible. As the flow profile is developed from the left side and we consider conduction at all boundaries of the porous-medium domain, a spatial variation in isotopic composition can be observed. As seen in the vertical isotopic profiles, the isotopic species are either enriched or depleted in the porous-medium

domain. During stage-I evaporation, the isotopologues enrich over the whole column width. As evaporation progresses, the upper layers of the porous-medium domain dries completely, and the isotopologues are depleted because the influence of the atmosphere with low isotopic concentration increase.

In our study, we analyze how the different stages of evaporation influences the enrichment of the water isotopologues. In Figure 4, the temporal isotopic composition evolution for different soil column depths and the corresponding evaporation rate are plotted. We can see that during stage-I evaporation, where evaporation rates are higher, the isotopic composition first enriches before depletion. This enrichment peak is here referred to as "stage-I peak". Afterwards, during the transition to stage-II evaporation, we observe another peak in isotopologue composition, which we refer to as "stage-II peak".

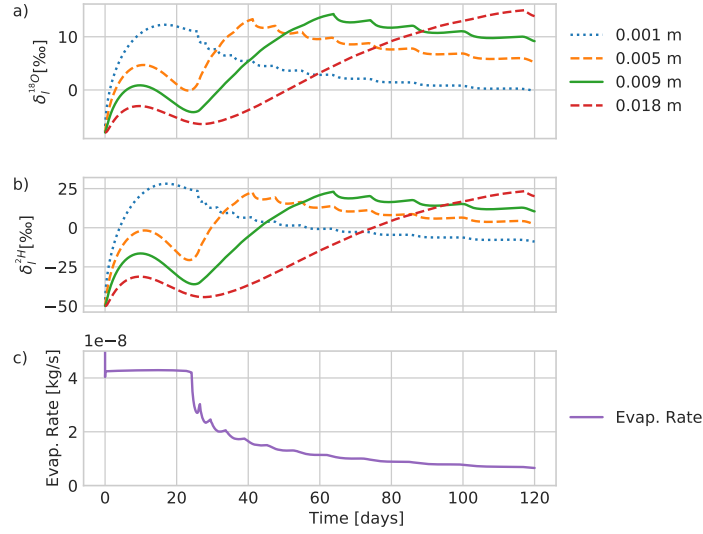


Figure 4: Influence of evaporation behaviour on the isotopic fractionation process in different soil column depths over time. (a),(b) Isotopic composition δ_i^j ; (c) evaporation rate over a 120 day period.

During stage-I evaporation, the isotopologues first enrich due to their lower vapor pressure relative to ordinary water. As the soil begins to dry, the isotopic composition decreases as isotopologue-depleted air from the atmosphere intrudes into the drying soil. At a certain state of drying the porous medium reaches the residual saturation. With no mobile liquid water at the surface, further evaporation is limited by vapor transport in the gas phase. Compared to before, isotopic species are enriching again, leading to a second peak. In this stage, the intrusion of air from the atmosphere is decreasing, as the air volume in the porous medium does not change very much anymore. However, lighter water isotopologues are still evaporating from the remaining liquid water, resulting in an increase in the isotopic composition. This leads to the second peak, the "stage-II peak". When drying further, eventually the water saturation reaches zero and the isotopologue composition decreases again.

These peaks in isotopologue composition are also described in various other modeling studies, e.g. for unsaturated soils by Barnes and Allison (1983). In their study they consider a soil with a dry layer on top, that is dominated by vapor transport. This described peak corresponds to our "stage-II peak" mentioned in this work.

In Figure 4, we show that the isotopic composition over time for various depths can be used to gain further insights into the evaporation and isotopologue transport processes. In the first soil layer, we only observe a stage-I peak. As this cell is located at the interface, the cell directly dries out when the atmospheric demand can no longer be supplied. In the other depths, the impact of the transition between stage-I and stage-II evaporation becomes more visible. However, with increasing soil depths, the evolution of the stage-I peak becomes less dominant as soils further from the surface are less impacted by the atmospheric evaporation demand.

4.2 Study of fractionation process

Mathieu and Bariac (1996) proposed a qualitative study to validate the isotopic enrichment of their isotope transport model. The aim of this study was to check on the influencing fractionation parameters by isolating each specific parameter. In Table 2, the isolated parameters used in the model for this processes study are summarized. Note that all parameters are listed given a temperature of 289K.

Table 2: Parameter change for fractionation process study

Case	Description	Gas pressure p^i	Gas diffusion coeff. $D_g^{i,air}$	Liq. diffusion coeff. $D_l^{H_2O,i}$	Mole fraction in Ω_{ff}
1	No fractionation	p^{H_2O}	$D_g^{H_2O,air}$	$D_l^{H_2O,self}$	$x_{g,ff}^i = x_{g,pm}^i$
2	Only equilibrium fractionation	p^i	$D_g^{H_2O,air}$	$D_l^{H_2O,self}$	$x_{g,ff}^i = x_{g,pm}^i$
3	Only kinetic fractionation	p^{H_2O}	$D_g^{i,air}$	$D_l^{H_2O,self}$	$x_{g,ff}^i = x_{g,pm}^i$
4	Surface depletion	p^{H_2O}	$D_g^{H_2O,air}$	$D_l^{H_2O,self}$	$x_{g,ff}^i < x_{g,pm}^i$
5	Only liquid diffusion	p^{H_2O}	$D_g^{H_2O,air}$	$D_l^{H_2O,i}$	$x_{g,ff}^i = x_{g,pm}^i$
6	Reference	p^i	$D_g^{i,air}$	$D_l^{H_2O,i}$	$x_{g,ff}^i < x_{g,pm}^i$

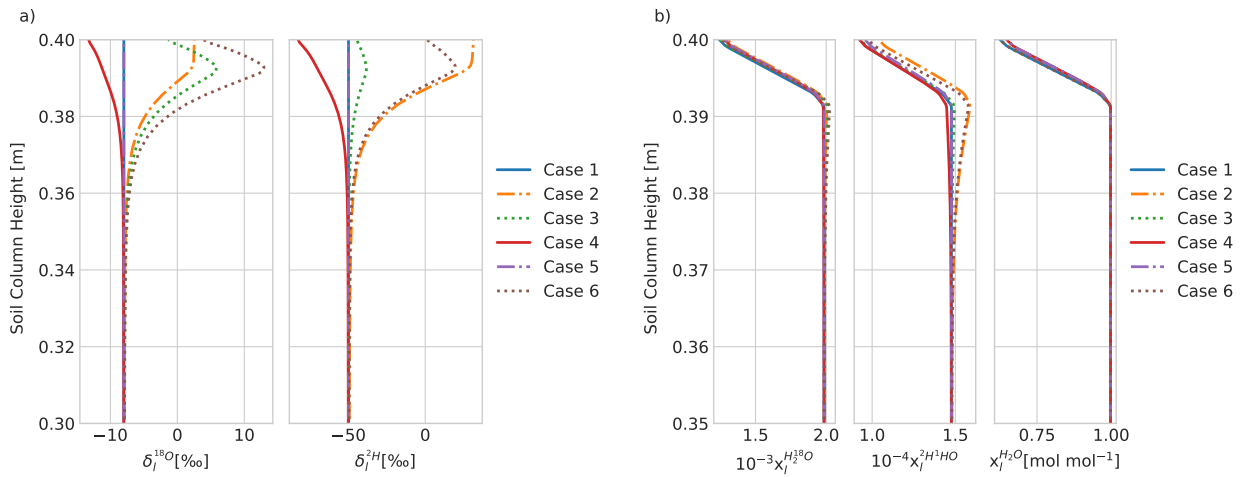


Figure 5: Process behaviour of isolated fractionation parameter at 50 days. (a) Isotopic composition δ_l^i ; (b) mole fraction x_l^κ of ordinary water and its isotopes.

In Figure 5 the results of our fractionation study are displayed. The fractionation process is analyzed for the vertical isotope profiles for $^2H^1HO$ and $H_2^{18}O$. The study cases are performed with the same model setup as described in Section 3, and with the same drying conditions ($v_x = 0.1$ m/s, 50 day period). Additionally, we compare the isotope profiles with the mole fractions of water and its isotopologues in the liquid phase to enhance our understanding of fractionation processes. It can be seen that the fractionation process is not as obvious in the mole fraction formulation as in the delta notation.

- **Case 1 - No isotopic fractionation:** All factors which lead to isotopic fractionation (vapor pressure difference, liquid and gaseous diffusion coefficients, isotopic composition gradient between free-flow and porous-medium domain) are neutralized. Hence, no significant fractionation compared to the initial state are obtained (max. deviation for $H_2^{18}O < 0.199\%$ and for $^2H^1HO < 0.030\%$). As we are observing an evaporation process, a concentration gradient towards the soil surface is formed (vapor zone). However, as water and its isotopes are both evaporating with the same slope, the isotopic composition remains constant.
- **Case 2 - Only equilibrium fractionation:** The equilibrium fractionation factor describes the tendency of a component to separate from a mixture. In our case, $^2H^1HO$ is more likely to partition from ordinary water than $H_2^{18}O$ ($\alpha_{eq}^{^2H^1HO} = 0.921$, $\alpha_{eq}^{H_2^{18}O} = 0.990$). By enabling the difference in vapour pressure of the isotopes, the equilibrium fractionation is reintroduced ($p_g^{H_2O} = 1801.4Pa$, $p_g^{^2H^1HO} = 1659.88Pa$, $p_g^{H_2^{18}O} = 1782.51Pa$). The isotopologues enrich towards the evaporation front due to phase equilibrium conditions. In the vapour zone the composition remains constant since the domain has switch into a one-phase system. Thus no equilibrium fractionation due to phase changes occurs in this zone.
- **Case 3: Only kinetic fractionation** Compared to Case 1, the binary gas diffusion coefficient is reintroduced for the isotopologues ($D_g^{H_2O,air} = 2.36e^{-5}m^2s^{-1}$, $D_g^{^2H^1HO,air} = 2.30e^{-5}m^2s^{-1}$, $D_g^{H_2^{18}O,air} = 2.29e^{-5}m^2s^{-1}$). Enabling the gas diffusion coefficient leads to an increase in the unsaturated zone as the isotopologues diffuse slower due to the lower diffusion coefficient, and subsequently to an decrease in the gaseous zone towards the isotopic-depleted free-flow concentration.
- **Case 4 - Only surface depletion:** Here, the influence of the depleted atmospheric conditions ($\delta_g^{^2H} = -100\text{‰}$, $\delta_g^{H_2^{18}O} = -16\text{‰}$) are analyzed. As drying proceeds, the isotopic concentration within the porous medium tends to the isotopic concentration in free flow.
- **Case 5 - Only liquid diffusion coefficient:** The liquid diffusion coefficient of the isotopologues is proportional to the self diffusion coefficient of pure water ($D_l^{H_2O,i} = a^i D_l^{H_2O,self}$) (Mathieu & Bariac, 1996). As the liquid diffusion may influence the mixing behavior of the isotopologues in the saturated and unsaturated zone, we isolate the liquid diffusion coefficient instead of only using the self-diffusion coefficient of water for the isotopic species ($D_l^{H_2O,self} = 1.819e^{-9}m^2s^{-1}$, $D_l^{^2H^1HO} = 1.789e^{-9}m^2s^{-1}$, $D_l^{H_2^{18}O} = 1.759e^{-9}m^2s^{-1}$). The liquid diffusion coefficient itself does not majorly affect the fractionation process as the advective term dominates the mixing and flow process in this case (compared to the initial state max. deviation for $H_2^{18}O < 0.122\%$ and for $^2H^1HO < 0.019\%$).
- **Case 6 - Reference:** As a reference, we enable all factors leading to fractionation. The results show both, a high enrichment towards the evaporation front (as in Case 2) and a depletion towards the soil surface (Case 3 + 4).

4.3 Variation of free-flow domain model

In the previous sections, investigations have been focused to laminar flow problems. However, when considering realistic atmospheric conditions with higher wind velocities, turbulent flow conditions must be regarded as well. As stated above, many studies have been focused on integrating turbulent mixing into the isotopic fractionation process by adapting the kinetic fractionation factor (e.g. Quade et al., 2018). By changing our free flow - porous medium coupled transport model by using the Reynold's averaged Navier-Stokes (RANS) equations and choosing a $k-\omega$ -model turbulence model as described in Section 2 and in (Heck et al., 2020; Coltman et al., 2020), we can affect the kinetic fractionation process at the interface region.

The velocity profile in the free-flow domain evolves from left to right from a block velocity profile to a fully developed flow profile for turbulent flow. For the laminar cases, a parabolic velocity profile is set on the left side, and from that, the flow profile develops. In Figure 6 the different flow scenarios are schematically displayed. The different flow scenario affect the diffusive flux near the interface, which further influence the evaporation rate at the soil surface (Figure 7) and so the isotopic fractionation behaviour inside the porous medium (Figure 8). As we want to show the variety of our free-flow model, we chose realistic flow scenarios for our laminar and turbulent flow cases. Since laminar flow mostly occurs indoors or under controlled conditions the boundary conditions for the laminar case resemble a wind tunnel. As the isotopic fractionation is an environmental issue, we are also interested in outdoor conditions. Therefore, we choose for the turbulent case boundary conditions which are suitable to replicate outdoor conditions, without a closed top at the upper boundary.

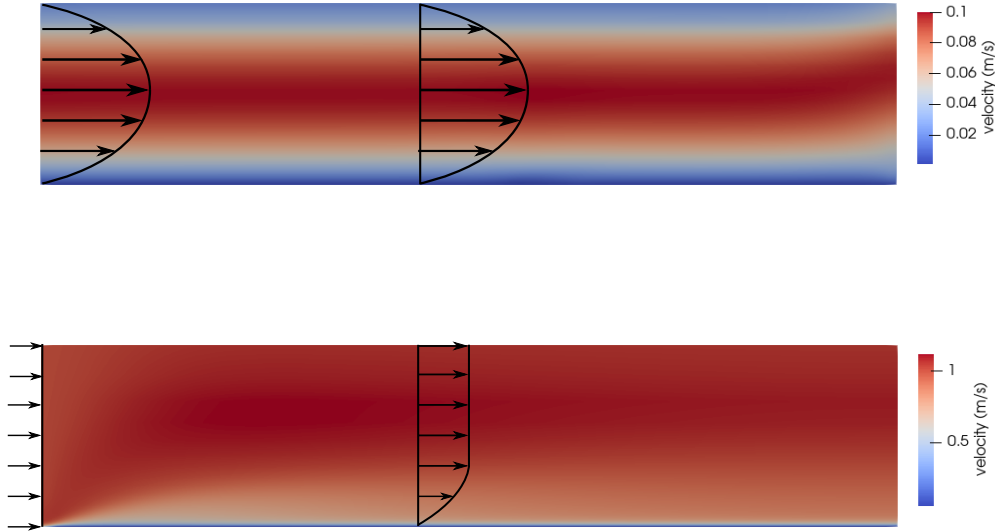


Figure 6: Influence of the boundary layer thickness developed by (a) laminar, (b) turbulent flow on mass transfer at the interface. We assume that the mass transfer is limited at the interface region, boundary layers form based on the present flow type and that outside the formed boundary layer the flow is fully mixed.

For our analysis of the influence of different flow conditions on fractionation processes, we test different free-flow velocities (Table 3). The turbulent flow problems result in different evaporation rates and evaporation profiles (Figure 7), as the maximum

386 evaporation rate is higher and the duration of stage-I is shortened by increasing the flow
 387 velocity.

Table 3: Turbulence parameter. (For parabolic flow profiles, the characteristic length of the Reynolds number (Re_D) is the diameter of the wind tunnel ($d=0.25\text{m}$) and for initial block profile flow (Re_L), we use the length between the starting point of the free-flow domain and the porous-medium domain ($l = 0.6 \text{ m}$).)

Case	Conditions	Flow Velocity [ms^{-1}]	Reynolds Number [-]
1	Laminar	0.1	$Re_D = 1\,678$
2	Laminar	0.13	$Re_D = 2\,181$
3	Turbulent	0.5	$Re_L = 2.01\text{e}4$
4	Turbulent	1.0	$Re_L = 4.03\text{e}4$
5	Turbulent	3.0	$Re_L = 1.21\text{e}5$

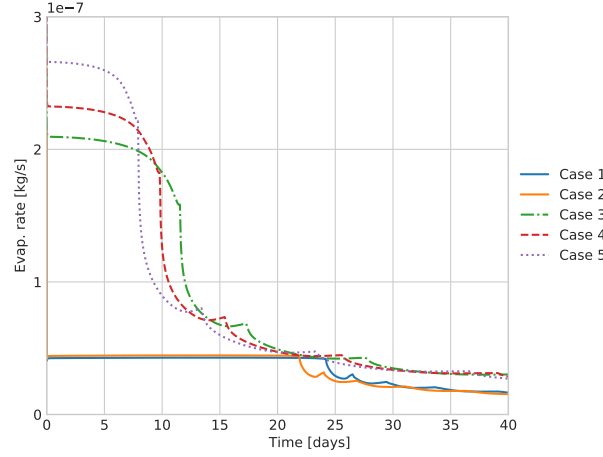


Figure 7: Evaporation rates over time for turbulent (dashed) and laminar (straight) flow problems

388 In the previous section, we hypothesized that the stage of evaporation (stage-I/stage-
 389 II) will have a crucial influence on the isotopic fractionation behavior in the porous medium.
 390 Thus, we analyze the isotopic distribution (in the vertical and horizontal direction) dur-
 391 ing different evaporation states and for different velocities (Figure 8). We compare the
 392 different flow cases among each other during stage-I and stage-II and for the transition
 393 zone between those stages. With this in mind, simulation times are selected such that
 394 all cases reached similar evaporation stages. However, due to the great difference in evap-
 395 oration rates, it is not possible to separate the stages for all cases completely.

396 Vertical isotopic distribution

- 397 • **Stage-I Evaporation:** In this stage, the isotopic fractionation is characterized
 398 by equilibrium fractionation. Whereas the turbulent and laminar flow problems
 399 behave very similarly, laminar cases enrich less towards the soil surface, but show

a greater difference in isotopic composition and a higher isotopic gradient. This is due to the higher evaporation rates seen in the turbulent cases. Thus the influence of the equilibrium fractionation is reduced and therefore less difference in the isotopic composition. However, some differences are still visible; The highest velocities lead to the highest enrichment. A reason for this is the different temperatures during stage-I evaporation. Higher evaporation rates lead to substantial evaporative cooling. The equilibrium fractionation process is very temperature sensitive and lower temperatures lead to lower equilibrium fractionation factors which means more partitioning of the isotopologues.

- **Transition:** A mixed representation of different evaporation states is visible at this point in the simulation. Where the laminar cases are still in stage-I evaporation, the turbulent cases are in different stages of the transition into stage-II evaporation. Thus, the interpretation of the turbulence impact on the isotopic composition in this zone is not absolute, but we regard one representative time. However, in all three turbulent cases, we observe that near the soil surface (0.39-0.38 m) the peak in isotopic composition has decreased in comparison with stage-I evaporation.

While in the transition zone, the soil temperature raises again due to lower evaporation rates and less evaporative cooling. Then the equilibrium fractionation does not affect the isotopic composition that much anymore and kinetic fractionation becomes more dominant.

Since the laminar cases are still in stage-I evaporation, the isotopic fractionation behavior remains similar to the previous stage. However, one may notice that the surface isotopic composition is increased as was observed in the turbulent cases (see Figure 8a). The wind velocities affect the speed of enrichment at the soil surface and the drying of the porous medium but does not significantly affect the maximum isotopic composition at the surface.

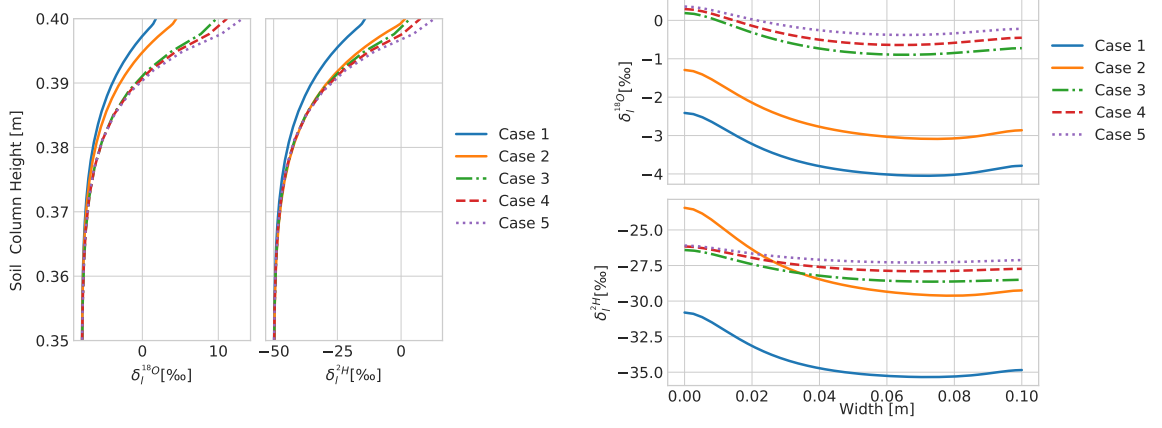
- **Stage-II Evaporation:** Here, all cases are in stage-II evaporation and all cases has developed the characteristic peak of the isotopologues. The turbulent cases show a very similar behaviour. Only minor deviations in the maximal enrichment are visible. For laminar flow, we observe that the maximum enrichment is greater for higher wind velocities, while the evaporation front is nearly on the same level. Still, higher wind velocities lead to drier soil, which in turn effects the peak in isotopic composition.

Horizontal isotopic distribution

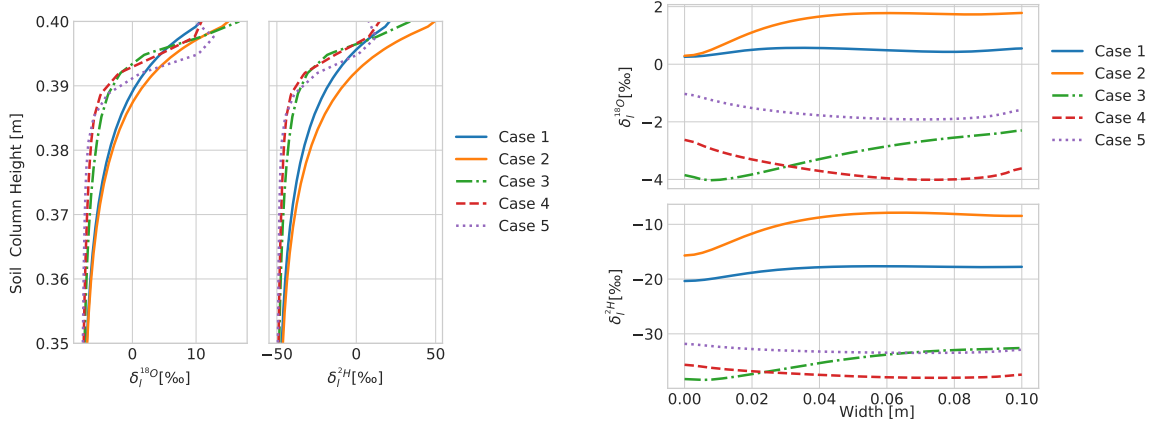
The impact of the varied free-flow conditions and the subsurface thermal boundary conditions can be observed by evaluating the spatial distribution of the isotopic composition at different depths parallel to the interface.

The influence of the different wind velocities is visible in terms of the evolution of isotopic composition. As observed in the vertical profiles, the enrichment in the turbulent cases proceeds faster than the laminar cases. Again, the influence of the different evaporation stages of the different flow problems is visible. In stage-I and stage-II the isotopic composition increases, whereas the isotopic composition is decreasing in the transition zone. During stage-I and stage-II the isotopic composition of the turbulent cases show only minor deviations in comparison with the laminar cases. While in the transition zone, in which the evaporation state may varies for each case, the spatial distribution of the turbulent cases is also varying considerably. Here, the spatial isotopic composition of a developed evaporation front (Case 5), a forming evaporation front (Case 4), and a surface evaporation front (Case 3) are displayed. Further, the effects of decreasing evaporation rates and less evaporative cooling on the horizontal distribution of the isotopic composition during different evaporation steps can be observed here.

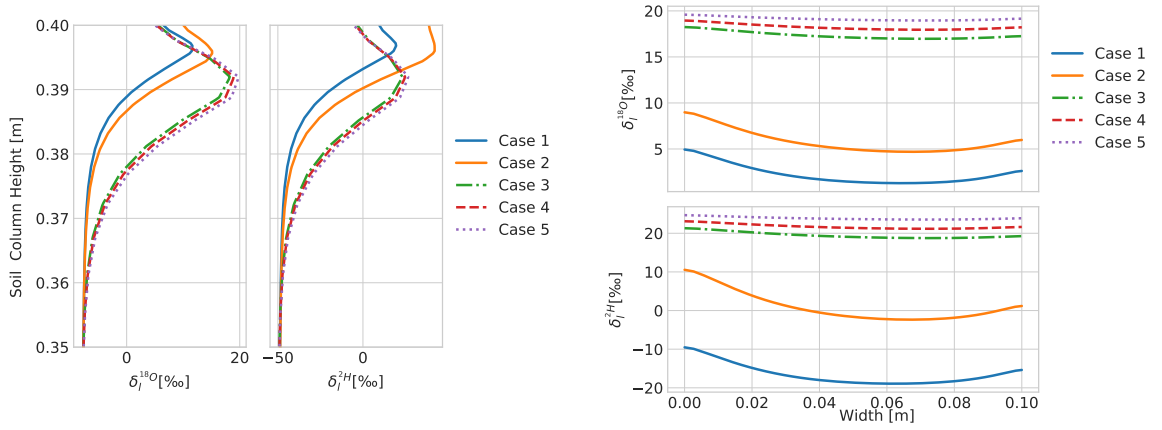
451 Considering the spatial variation of the isotopic enrichment within the single cases,
452 the one-dimensional assumption is for most cases sufficient. In addition, the applied con-
453 duction boundary condition in the porous medium of our virtual case has also a crucial
454 impact on the enrichment of the isotopologues. For special cases, as observed in our lam-
455 inar cases, a larger change in isotopic composition is possible along the horizontal axis.



(a) Stage-I evaporation ($t=2$ days)



(b) Transition evaporation ($t=10$ days)



(c) Stage-II evaporation ($t=35$ days)

Figure 8: Spatial isotopic composition in porous-medium domain for different flow problems (Laminar: Case 1,2 (solid lines); Turbulent: Case 3,4,5 (dashed lines)). Shown are vertical ($x = 0.05$ m) and horizontal ($y = 0.39$ m) isotopic profiles for different evaporation states.

5 Conclusion and Outlook

With the coupled model concept presented in this work, the transport and fractionation of stable water isotopologues during soil-water evaporation can be described. We solve transport equations for ordinary water, its isotopologues, and dry air in the porous medium and the free flow and use suitable coupling conditions to describe the mass, momentum, and energy conservation between the domains. In contrast to other existing models, further parameterization of the kinetic fractionation is not necessary as the transport and mixing in the system is modelled directly.

Considering laminar conditions, it is shown that the coupled model can reproduce the characteristic enrichment peaks in isotopic composition during the evolution of the evaporation front, as well as the depletion of isotopologues in the dry soil during the drying of the soil. Further, a correlation between the isotopic composition and the different stages of evaporation can be observed. In the isotopic composition at certain levels the impact of the different stages of evaporation is visible as during stage-I a first peak in the isotopic composition is observed and a second peak appears in stage-II evaporation. In an additional study, we test the robustness of our model by separating the processes of equilibrium and kinetic fractionation. The effect of wind velocity and turbulent mixing on the isotopic composition in soil is studied. For that, we use a RANS approach for the description of the turbulent flow in the free-flow. This analysis allows us to further study the influence of the evaporation rate and the evaporation stages on the isotopic composition. The temperature-sensitive equilibrium fractionation is affected by higher evaporation rates as less evaporative cooling leads to a higher partitioning of isotopologues. In stage-II evaporation, where the kinetic fractionation is more dominant, we observe a variation in the isotopic compositions of the different flow conditions: The turbulent flow cases have similar characteristic peaks in the isotopic composition, but the laminar flow cases show a greater influence of the wind velocity on the isotopic transport. The analysis in this work has shown that the coupled transport model can be used as a supportive tool to further specify the parametrization of kinetic fractionation.

Besides wind velocity and turbulent mixing in the free flow, other free-flow properties such as radiation and surface topology have a crucial impact on the fractionation in soils and at the soil-atmosphere interface. In (Heck et al., 2020) and (Coltman et al., 2020) it is presented how radiation and surface topology can be implemented in similar transport models. Additionally, the presence of salt concentration in soil waters affects the evaporation rate and so the fractionation process (Sofer & Gat, 1975), as salt precipitation and concentration instabilities occur during the evaporation process in the porous medium (Shokri-Kuehni et al., 2020). The effect of salinity on the fractionation process could be further investigated in the context of this model.

6 Open Research

All code relevant to obtaining the numerical examples is implemented in DuMux (Koch et al., 2021) and can be found under Gitlab (git.iws.uni-stuttgart.de/dumux-pub/Kiemle2022a).

Acknowledgments

We thank the Deutsche Forschungsgemeinschaft (DFG, German Research Foundation) for supporting this work by funding SFB 1313, Project Number 327154368 and the DFG Research Group Satin 2531/14-1. We also thank the DFG for supporting this work by funding SimTech via Germany's Excellence Strategy (EXC 2075 – 390740016).

References

Aleinov, I., & Schmidt, G. (2006). Water isotopes in the GISS modelE land surface

- scheme. *Global and Planetary Change*, 51, 108-120. doi: 10.1016/j.gloplacha.2005.12.010
- Barnes, C., & Allison, G. (1983). The distribution of deuterium and ^{18}O in dry soils: 1. Theory. *Journal of Hydrology*, 60(1-4), 141-156. doi: 10.1016/0022-1694(83)90018-5
- Barnes, C., & Allison, G. (1984). The distribution of deuterium and ^{18}O in dry soils: 3. Theory for non-isothermal water movement. *Journal of Hydrology*, 74(1-2), 119-135. doi: 10.1016/0022-1694(84)90144-6
- Beavers, G. S., & Joseph, D. D. (1967). Boundary conditions at a naturally permeable wall. *Journal of Fluid Mechanics*, 30(1), 197-207. doi: 10.1017/s0022112067001375
- Braud, I., Bariac, T., Gaudet, J. P., & Vauclin, M. (2005). SiSPAT-Isotope, a coupled heat, water and stable isotope (HDO and H_2^{18}O) transport model for bare soil. part I. model description and first verifications. *Journal of Hydrology*, 309(1-4), 277-300. doi: 10.1016/j.jhydrol.2004.12.013
- Brutsaert, W. (1975). The roughness length for water vapor sensible heat, and other scalars. *Journal of Atmospheric Sciences*, 32(10), 2028 - 2031. doi: 10.1175/1520-0469(1975)032<2029:TRLFWV>2.0.CO;2
- Coltman, E., Lipp, M., Vescovini, A., & Helmig, R. (2020). Obstacles, interfacial forms, and turbulence: A numerical analysis of soil-water evaporation across different interfaces. *Transport in Porous Media*, 134. doi: 10.1007/s11242-020-01445-6
- Craig, H. (1961). Isotopic variations in meteoric waters. *Science*, 133(3465), 1702-1703. doi: 10.1126/science.133.3465.1702
- Craig, H., & Gordon, L. I. (1965). Deuterium and oxygen 18 variations in the ocean and marine atmosphere. Consiglio nazionale delle ricerche, Laboratorio de geologia nucleare Pisa.
- Dongmann, G., Nürnberg, H. W., Förstel, H., & Wagener, K. (1974). On the enrichment of H_2^{18}O in the leaves of transpiring plants. *Radiation and Environmental Biophysics*, 11, 41-52. doi: 10.1007/BF01323099
- Fetzer, T., Smits, K. M., & Helmig, R. (2016). Effect of turbulence and roughness on coupled porous-medium/free-flow exchange processes. *Transport in Porous Media*, 114(2), 395-424. doi: 10.1007/s11242-016-0654-6
- Flemisch, B., Darcis, M., Erbertseder, K., Faigle, B., Lauser, A., Mosthaf, K., ... Helmig, R. (2011). DuMux: DUNE for multi-phase,component,scale,physics,... flow and transport in porous media. *Advances in Water Resources*, 34(9), 1102-1112. (New Computational Methods and Software Tools) doi: https://doi.org/10.1016/j.advwatres.2011.03.007
- Gat, J. R. (1971). Comments on the stable isotope method in regional groundwater investigations. *Water Resources Research*, 7(4), 980-993. doi: 10.1029/WR007i004p00980
- Gonfiantini, R. (1978). Standards for stable isotope measurements in natural compounds. *Nature*, 271(5645), 534-536. doi: 10.1038/271534a0
- Haese, B., Werner, M., & Lohmann, G. (2012). Stable water isotopes in the coupled atmosphere-land surface model echam5-jsbach. *Geoscientific Model Development*, 5, 3375-3418. doi: 10.5194/gmd-6-1463-2013
- Haverd, V., & Cuntz, M. (2010). Soil-Litter-Iso: A one-dimensional model for coupled transport of heat, water and stable isotopes in soil with a litter layer and root extraction. *Journal of Hydrology*, 388(3-4), 438-455. doi: 10.1016/j.jhydrol.2010.05.029
- Heck, K., Coltman, E., Schneider, J., & Helmig, R. (2020). Influence of radiation on evaporation rates: A numerical analysis. *Water Resources Research*, 56. doi: 10.1029/2020WR027332
- Horita, J., & Wesolowski, D. (1994). Liquid-vapor fractionation of oxygen and hydrogen isotopes of water from the freezing to the critical temper-

- ature. *Geochimica et Cosmochimica Acta*, 58(16), 3425–3437. doi: 10.1016/0016-7037(94)90096-5
- IAPWS. (2007). *Revised release on the iapws industrial formulation 1997 for the thermodynamic properties of water and steam* (Tech. Rep. No. IAPWS R7-97(2012)). Lucerne, Switzerland: The International Association for the Properties of Water and Steam.
- Jiang, Z., Xu, T., Mallants, D., Tian, H., & Owen, D. (2018). Numerical modelling of stable isotope (2H and 18O) transport in a hydro-geothermal system: Model development and implementation to the guide basin, china. *Journal of Hydrology*. doi: 10.1016/j.jhydrol.2018.11.065
- Jones, I. P. (1973). Low Reynolds number flow past a porous spherical shell. *Mathematical Proceedings of the Cambridge Philosophical Society*, 73(1), 231–238. doi: 10.1017/S0305004100047642
- Koch, T., Gläser, D., Weishaupt, K., Ackermann, S., Beck, M., Becker, B., . . . Flemisch, B. (2021). DuMux 3 – an open-source simulator for solving flow and transport problems in porous media with a focus on model coupling. *Computers & Mathematics with Applications*, 81, 423–443. (Development and Application of Open-source Software for Problems with Numerical PDEs) doi: 10.1016/j.camwa.2020.02.012
- Kraft, P., Vaché, K., & Breuer, L. (2011). Cmf: A hydrological programming language extension for integrated catchment models. *Environmental Modelling & Software*, 26, 828–830. doi: 10.1016/j.envsoft.2010.12.009
- Kuppel, S., Tetzlaff, D., Maneta, M., & Soulsby, C. (2018). EcH2O-iso 1.0: Water isotopes and age tracking in a process-based, distributed ecohydrological model. *Geoscientific Model Development*, 11, 3045–3069. doi: 10.5194/gmd-11-3045-2018
- Lehmann, P., Assouline, S., & Or, D. (2008). Characteristic lengths affecting evaporative drying of porous media. *Phys. Rev. E*, 77, 056309. doi: 10.1103/PhysRevE.77.056309
- Luz, B., Barkan, E., Yam, R., & Shemesh, A. (2009). Fractionation of oxygen and hydrogen isotopes in evaporating water. *Geochimica Et Cosmochimica Acta - GEOCHIM COSMOCHIM ACTA*, 73, 6697–6703. doi: 10.1016/j.gca.2009.08.008
- Majoube, M. (1971). Fractionnement en oxygène 18 et en deutérium entre l’eau et sa vapeur. *J. Chim. Phys.*, 68, 1423–1436. doi: 10.1051/jcp/1971681423
- Mathieu, R., & Bariac, T. (1996). An isotopic study (2H and 18O) of water movements in clayey soils under a semiarid climate. *Water Resources Research*, 32(4), 779–789. doi: 10.1029/96WR02995
- Melayah, A., Bruckler, L., & Bariac, T. (1996). Modeling the transport of water stable isotopes in unsaturated soils under natural conditions: 1. theory. *Water Resources Research*, 32, 2047–2054. doi: 10.1029/96WR00674
- Merlivat, L. (1978). Molecular diffusivities of H_2^{16}O , HD^{16}O , and H_2^{18}O in gases. *The Journal of Chemical Physics*, 69(6), 2864–2871. doi: 10.1063/1.436884
- Moore, R. (1937). *Water conduction from shallow water tables*. University of California, Berkeley. doi: 10.3733/hilg.v12n06p383
- Mosthaf, K., Baber, K., Flemisch, B., Helmig, R., Leijnse, A., Rybak, I., & Wohlmuth, B. (2011). A coupling concept for two-phase compositional porous-medium and single-phase compositional free flow. *Water Resources Research*, 47(10). doi: 10.1029/2011wr010685
- Müller, M., Alaoui, A., Kuells, C., Leistert, H., Meusburger, K., Stumpp, C., . . . Alewell, C. (2014). Tracking water pathways in steep hillslopes by $\delta^{18}\text{O}$ depth profiles of soil water. *Journal of Hydrology*, 519, 340–352. doi: 10.1016/j.jhydrol.2014.07.031
- Quade, M., Brüggemann, N., Graf, A., Vanderborght, J., Vereecken, H., & Rothfuss, Y. (2018). Investigation of kinetic isotopic fractionation of water during

- bare soil evaporation. *Water resources research*, 54(9), 6909–6928. doi: 10.1029/2018WR023159
- Risi, C., Ogée, J., Bony, S., & Besson, C. (2016). The water isotopic version of the land-surface model orchidee: Implementation, evaluation, sensitivity to hydrological parameters. *Journal of Waste Water Treatment & Analysis*, 07. doi: 10.4172/2157-7587.1000258
- Rothfuss, Y., Merz, S., Vanderborght, J., Hermes, N., Weuthen, A., Pohlmeier, A., ... Brüggemann, N. (2015). Long-term and high-frequency non-destructive monitoring of water stable isotope profiles in an evaporating soil column. *Hydrology and Earth System Sciences*, 19(10), 4067–4080. doi: 10.5194/hessd-12-3893-2015
- Saffman, P. G. (1971). On the boundary condition at the surface of a porous medium. *Studies in Applied Mathematics*, 50(2), 93–101. doi: 10.1002/sapm197150293
- Shokri-Kuehni, S. M. S., Raaijmakers, B., Kurz, T., Or, D., Helmig, R., & Shokri, N. (2020). Water table depth and soil salinization: From pore-scale processes to field-scale responses. *Water Resources Research*, 56(2). doi: 10.1029/2019WR026707
- Shurbaji, A.-R. M., & Phillips, F. M. (1995). A numerical model for the movement of H₂O, H₂¹⁸O, and 2HHO in the unsaturated zone. *Journal of Hydrology*, 171, 125–142. doi: 10.1016/0022-1694(94)02604-A
- Sofer, Z., & Gat, J. (1975). The isotope composition of evaporating brines: Effect of the isotopic activity ratio in saline solutions. *Earth and Planetary Science Letters*, 26(2), 179–186. doi: 10.1016/0012-821X(75)90085-0
- Somerton, W., Keese, J., & Chu, S. (1974). Thermal Behavior of Unconsolidated Oil Sands. *Society of Petroleum Engineers Journal*, 14(05), 513–521. doi: 10.2118/4506-PA
- Sprenger, M., Leistert, H., Gimbel, K., & Weiler, M. (2016). Illuminating hydrological processes at the soil-vegetation-atmosphere interface with water stable isotopes. *Reviews of Geophysics*, 54(3), 674–704. doi: 10.1002/2015rg000515
- Sprenger, M., Tetzlaff, D., Buttle, J., Laudon, H., Leistert, H., Mitchell, C. P., ... Soulsby, C. (2018). Measuring and modeling stable isotopes of mobile and bulk soil water. *Vadose Zone Journal*, 17(1), 170149. doi: 10.2136/vzj2017.08.0149
- Stumpp, C., Stichler, W., Kandolf, M., & Simunek, J., Jiri. (2012). Effects of land cover and fertilization method on water flow and solute transport in five lysimeters: A long-term study using stable water isotopes. *Vadose Zone Journal*, 11, 0. doi: 10.2136/vzj2011.0075
- Uhlenbrook, S., Roser, S., & Tilch, N. (2004). Hydrological process representation at the meso-scale: The potential of a distributed, conceptual catchment model. *Journal of Hydrology*, 291, 278–296. doi: 10.1016/j.jhydrol.2003.12.038
- Van Hook, W. A. (1968). Vapor pressures of the isotopic waters and ices. *The Journal of Physical Chemistry*, 72(4), 1234–1244. doi: 10.1021/j100850a028
- Wilcox, D. C. (2008). Formulation of the k-w turbulence model revisited. *AIAA Journal*, 46(11), 2823–2838. doi: 10.2514/1.36541
- Windhorst, D., Kraft, P., Timbe, E., Frede, H.-G., & Breuer, L. (2014). Stable water isotope tracing through hydrological models for disentangling runoff generation processes at the hillslope scale. *Hydrology and Earth System Sciences*, 18, 4113–4127. doi: 10.5194/hess-18-4113-2014
- Wong, T., Nusbaumer, J., & Noone, D. (2017). Evaluation of modeled land-atmosphere exchanges with a comprehensive water isotope fractionation scheme in version 4 of the community land model. *Journal of Advances in Modeling Earth Systems*, 9. doi: 10.1002/2016MS000842
- Zhou, T., Simunek, J., Jiri, & Braud, I. (2021). Adapting HYDRUS-1D to simulate the transport of soil water isotopes with evaporation fractiona-

tion. *Environmental Modelling & Software*, 143, 105118. doi: 10.1016/
j.envsoft.2021.105118